Journal of Magnetism and Magnetic Materials 584 (2023) 171081

Contents lists available at ScienceDirect

Journal of Magnetism and Magnetic Materials

journal homepage: www.elsevier.com/locate/jmmm

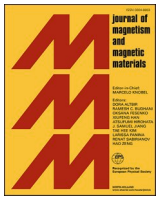

Research article

A model to account for magnetic permeability changes resulting from edge damage caused by laser cutting in a high performance cobalt-iron alloy

Xiao Chen [a,*], Han Wu [a], Jason D. Ede [a], Geraint W. Jewell [a], Luke M. Jones [b], Hassan Ghadbeigi [b]

[a] Department of Electronic and Electrical Engineering, University of Sheffield, Sheffield S1 3JD, United Kingdom
[b] Department of Mechanical Engineering, University of Sheffield, Sheffield S1 3JD, United Kingdom

ARTICLE INFO

Keywords:
Laser cutting
Edge damage effect
Cobalt-iron
Magnetic permeability reduction

ABSTRACT

Laser cutting is the mainstay of electrical machine stator core manufacture for prototyping and for high value, small and medium batch sizes. However, it can introduce localized damage into electrical steels, with reduction in magnetic permeability and increase in core loss in regions adjacent to the edge. These phenomena have been studied in Silicon-iron alloys, but there is little published data on Cobalt-iron. This paper presents experimental measurements on magnetic edge damage effect in Cobalt-iron alloys due to laser cutting. The paper then uses magnetic measurements for an increasing number of cuts in test samples to develop a model that represents the deterioration of magnetic permeability with distance from the cut edge, including cumulative damage effects from multiple cuts. The model is suitable for incorporation into finite-element models, either as a continuous function of position or to generate individual magnetization curves for discrete layers in finite-element mesh. The paper concludes by using the model to generate a series of magnetization curves which include the damage effect and in turn uses these to predict the net magnetic behavior of a series of rectangular strips. Good agreement is obtained between these predictions and measurements of samples from the same batch of Cobalt-iron.

1. Introduction

Laser cutting of electrical steel laminations is widely used in prototyping and low to medium volume manufacture of stator and rotor cores for electrical machines. Laser cutting offers a good balance of flexibility, throughput and little or no up-front tooling cost [1]. Despite the merits of stamping [2], abrasive water-jet cutting [3], wire electro-discharge machining [4], rotary cutting [5] and chemical etching [6], laser cutting remains the mainstay of high value, small and medium batch size electrical machine stator core manufacture. As the number of laminations of a given profile increases, there is a breakpoint beyond which lamination stamping with a high-speed press becomes more economical despite the initial outlay on geometry specific tooling. This breakpoint depends on a number of factors including the production volume, stamping tooling cost, tool lifetime, etc [7].

The functional magnetic properties of high-performance electrical steels rely on precise control of the microstructure during their manufacture. This makes electrical steels prone to localized degradation of the magnetic properties due to secondary process steps such as cutting [8–11], welding [12] or shrink-fitting of cores into housings [13]. In combination, these various processes contribute to the notion of a 'build-factor' for a finished core in which some discounting of the nominal magnetic properties of the starting material is assumed to occur in the final assembled machine. This is often based on empirical factors arrived at through accumulated experience. Of the many processes which can degrade the magnetic properties edge damage during cutting can be a significant contributor to the overall build-factor.

Edge damage can manifest itself as both a reduction in permeability near the cut edge, which in turn results in a degree of flux redistribution within the core [14], and as a localized change in loss of the core material [15]. It is worth noting that the degree of flux redistribution is dependent on the flux density level in the core, being least pronounced with the onset of significant magnetic saturation throughout the core. Measurements to characterize the nature of the edge damage on test samples provide a useful insight into the underlying behavior and some guidance on process optimization. However, to quantify the effect on the performance of given machine, necessitates a further challenging step of linking of this phenomenon to machine level models which are usually based on finite element modelling.

There is a growing body of literature on modelling permeability

* Corresponding author.
E-mail address: xiao.chen@sheffield.ac.uk (X. Chen).

https://doi.org/10.1016/j.jmmm.2023.171081
Received 9 May 2023; Received in revised form 11 July 2023; Accepted 25 July 2023
Available online 26 July 2023

reduction and core loss increase due to edge damage effects. Three types of models have been developed, including single layer material model [16,17], multi-layer material model [18,19], and continuous material model [10,20–22]. For single layer material models proposed in [16,17], a single region near to the cut edge to represent the edge damage region in which the DC magnetization curve has deteriorated was used. This type of model has a very limited degree of freedom to represent the edge damage effect on permeability reduction which should be a continuous variation with the distance to the cut edge.

The multi-layer material model, proposed in [16] employed multi-layer edge damage regions with various DC magnetization curves to facilitate the modelling of the permeability reduction due to edge damage. A nonuniform multi-layer edge damage effect model was further developed in [19]. However, this method assumes there is a clear boundary for the deteriorated zone while the deteriorated zone can cover the total width of the sample as reported in [23,24].

Various types of continuous material model were proposed in [10,20–22], using various continuous functions to represent the permeability change with respect to the distance to the cut edge. These continuous material models can be incorporated into finite element models by either multi-layer geometrical regions with various DC magnetization curves or one geometrical region with each mesh element being assigned a DC magnetization curve which is a function of the distance from the cut edge. However, to the best of the authors' knowledge, no paper has accounted for the magnetic field strength effect and the accumulative edge damage effect simultaneously.

This paper proposes a double exponential term edge damage effect model to account for the permeability changes in Cobalt-iron alloys due to laser cutting. Compared to the existing models in literature, the proposed model accounts for the magnetic field strength effect and the accumulative edge damage effect from multiple cuts simultaneously. The proposed model can be implemented by either multi-layer material model or continuous material model in finite element analysis.

2. Material testing

A. *Introduction*

Conventional magnetic test methods for bulk soft magnetic alloys include testing of toroid, single-strip, single-sheet or Epstein Frame samples. In order to ensure some degree of consistency and transferability, these test methods have protocols and sample specification set out in standards such as IEC 60404-2, IEC 60404-3 and IEC 60404-4. However, they all involve some degree of assumption to convert sample and test-rig specific measurements of coil flux-linkage, and in some cases excitation current, to general material characteristics. From the perspective of characterizing edge damage, a major limitation of these methods is that the flux density is an inferred mean quantity derived from a measurement of search coil flux-linkage with appropriate scaling for coil properties and sample dimensions. Such methods are based on ascribing a single mean value of flux density to a sample at a particular value of applied field strength with no means of determining the spatial variation.

The underlying assumption in these standard measurement methods is that the magnetic field within a sample is homogeneous in nature and the region of interest is at a single magnetic operating point. Hence, standard measurement methods are by their very underpinning definitions, incompatible with the need to measure localized magnetic effects within a sample. Whereas it is possible to measure the influence of different sample dimensions on the mean inferred properties, e.g., measuring toroidal samples of different widths, such an approach does not in itself establish quantitatively the nature of the variation in damage in the vicinity of the cut edge. The approach adopted in this study is to use a recognized test-method, in this case a single-strip test fixture, to measure average flux density and to use this data to parameter fit a model which accounts for spatial variation in magnetic properties.

B. *Test material and microstructural characterization*

A batch of Hiperco 50 Cobalt-iron strips were prepared by Carpenter Technology. The strips were nominally 0.15 mm thick, 30 mm wide and 300 mm long and samples were cut by blanking prior to heat treatment and subsequent magnetic characterization. The samples were heat-treated after blanking in line with the schedule specified for optimizing magnetic properties, i.e. heat treatment at ~870 °C. Two types of strips were cut, firstly with the 300 mm dimension parallel to the rolling direction (designated as RD samples) and secondly transverse to the rolling direction (designated as TD samples).

To investigate the effect of heat treatment and laser cutting on the microstructural morphology and chemical composition of the samples at the cut edge, a set of samples with shear cut edges and laser cut edges were hot mounted in conductive Bakelite. The samples were located to enable the analysis of the cut section. Standard metallography practice, ground and polished using P1200 and P2500 silicon carbide abrasive paper, followed by 6 μm, 1 μm, and 0.5 μm diamond suspensions, was followed to achieve a mirror polish on the regions of interest. Subsequently, the polished samples were swab etched with 6% Nital solution (6% by volume nitric acid of concentration 68%, balance industrial methylated spirits). After etching the images were acquired using bright-field microscopy with a 20x objective and a ZEISS Axiocam 105.

Fig. 1 shows the bulk microstructure of the material in the as-received condition (i.e. after the heat treatment) where grains with a diameter 13–150 μm can be observed. The bright strips in the figure are cross section of the material moulded in Bakelite (the black region of the micrograph). The micrograph shows grains as large as 150 μm surrounded by smaller grains due to variation of grain growth rate during the production cycles. The grain boundaries are revealed as narrow line in the strips as a result of the etching process. The microstructure of the shear and laser cut edges are shown in Fig. 2. While the applied cutting operations do not significantly alter the microstructural morphology at the vicinity of the cut edge, conventional features including roll over, shear and fracture zones and burr formation are visible in Fig. 2a. The highlighted region of the figure also demonstrates that although the localized shear bands are only visible to depth of about 50 μm, grains as deep as 100 μm are affected by the rollover region. Fig. 2b shows that the laser cutting process results in a straight edge with no visible heat affected zone (HAZ), however, given the thermal energy input to the material a very narrow thermally affected zone is expected that the associated investigations are out of the scope of this paper. Therefore, the effect of post shear cutting heat treatment and laser cutting on the microstructural morphology of the material was found to be negligible.

The cut edge topography of the samples was also investigated using Scanning Electron Microscope (SEM) micrographs and energy-dispersive X-ray (EDX) analysis was applied to determine the chemical composition of the material at various locations across the surface and cut edge. To measure the chemical composition before and after laser cut, 1 cm^2 samples with a shear and laser cut edge were produced by cutting with standard scissors. Samples were mounted on a 45° fixture such that the cut edge and top surface were visible. Several Energy Dispersive Spectroscopy (EDS) point spectra were acquired and the range of chemical elements were calculated for each case. Fig. 3 shows the SEM micrographs of the shear (Fig. 3a) and laser (Fig. 3b) cut samples where the relevant SEM imaging parameters are also indicated in the figures. The cut edge morphology for the shear cut sample clearly demonstrates shear and fracture zones with the flat and dimpled regions, respectively. The features on the cut edge of the laser cut sample, Fig. 3b, correspond to the kerfs of the laser cutting process that are spaced approximately 30–35 μm apart.

Table 1 and Table 2 list the ranges of elemental compositions at the very surface for shear and laser cut edges, respectively, obtained by the EDX analysis. It was found that, although no HAZ was observed at the cross-section, laser cut samples are marginally depleted from main alloying elements of Fe and Co, probably due to the formation of other

Fig. 1. Micrograph of the bulk material away from the cut edge showing a variation grain sizes as large as 150 μm.

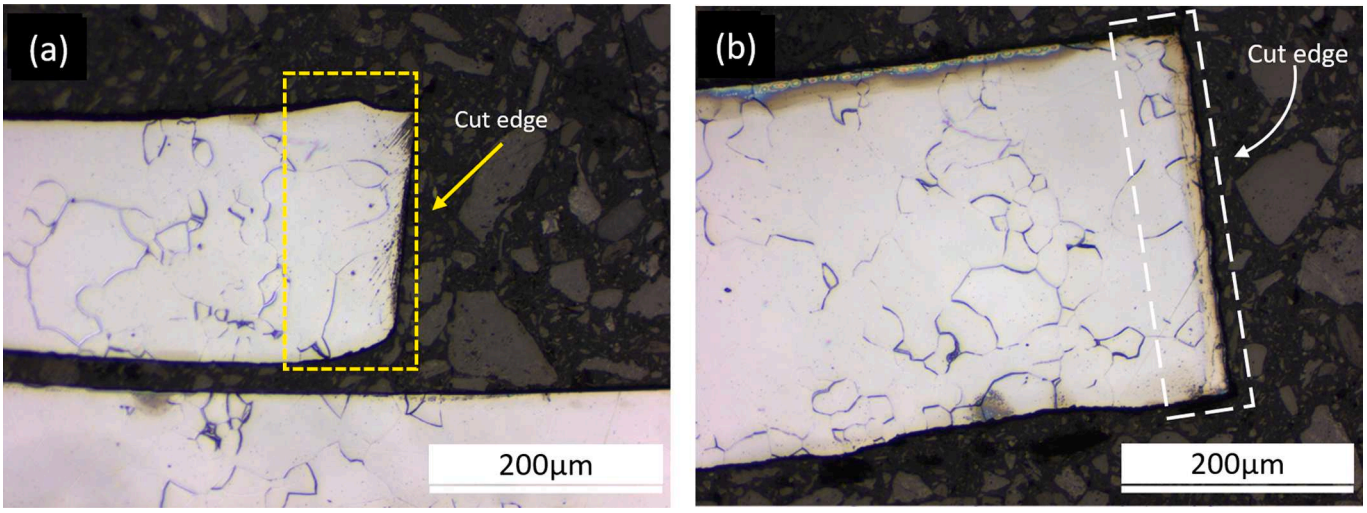

Fig. 2. Microstructural morphology of the cross section as the cut edge for (a) shear cut and (b) laser cut edges showing no significant alterations due to the cutting processes.

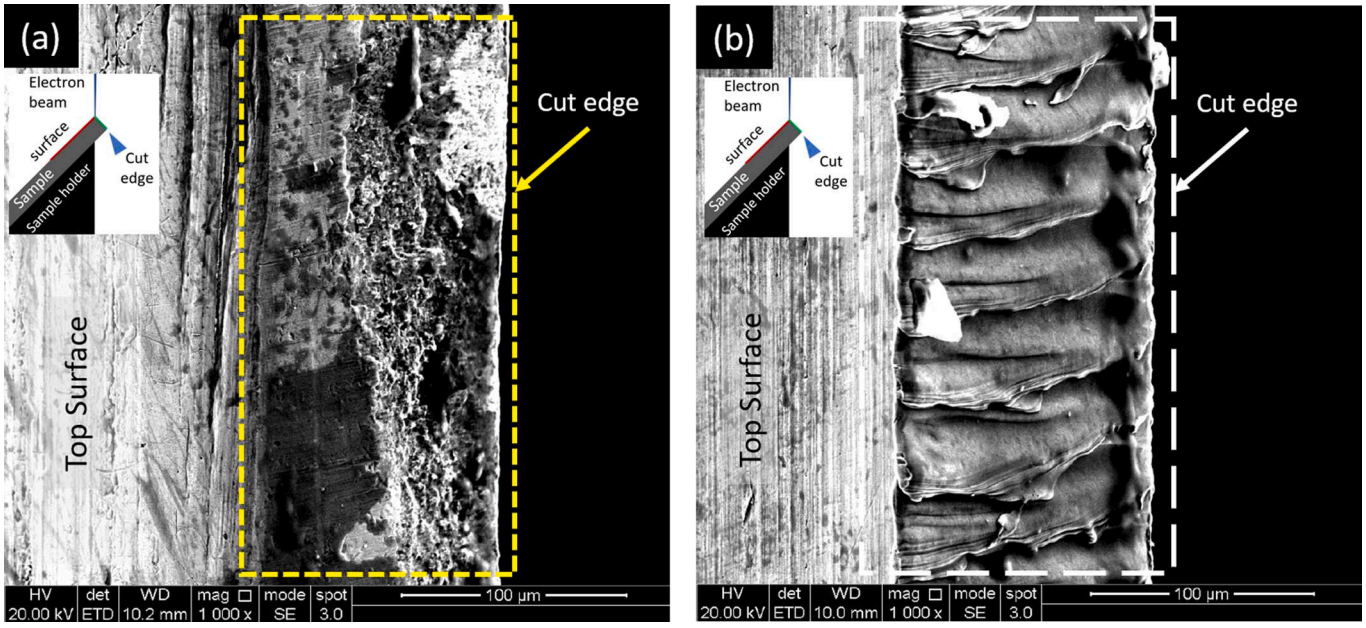

Fig. 3. Micrographs of the cut edge after (a) shear cutting and (b) laser cutting showing shear and fracture regions due to the shear cutting and the kerfs on the laser cut surface.

Table 1
Range of elemental compositions for shear cut edges.

Element	Percentage
Fe	42.2%–49.9%
Co	40.0%–56.4%
Al	0.0%–10.0%
V	0.6%–3.1%
O	0.0%–6.5%

Table 2
Range of elemental compositions for laser cut edges.

Element	Percentage
Fe	42.9%–46.8%
Co	41.0%–45.7%
Al	4.9%–6.4%
V	1.8%–2%
O	0.0%–6.4%

compounds on the surface during the laser cutting. The unexpected presence of aluminium may be due to contamination by the insulating panels used in laser cutting.

C. *Magnetic characterization*

Prior to any laser cutting, magnetic characterization of these samples was performed to provide a baseline against which any deterioration in properties could be subsequently assessed. The characterization was performed using a commercial single-strip test fixture (Laboratorio Elettrofisico ST-100) which has a sample distance between the yokes of 108 mm in combination with a Laboratorio Elettrofisico AMH-1K permeameter system, as shown in Fig. 4. Although this type of single strip tester is recognized as providing a measurement of magnetic properties with less absolute accuracy compared to an Epstein Frame, it provides a convenient means of assessing a large number of strips which have relative variations of magnetic properties due to any treatment between two measurements [25].

A total of 16 samples (8 rolling direction and 8 transverse direction) were initially characterized. The resulting mean maximum and minimum quasi-static magnetization curves from these batches are shown in Fig. 5(a) for both rolling (RD) and transverse (TD) directions. Fig. 5(b) shows their hysteresis loops at 400 Hz. As will be apparent, there is a significant difference in the magnetization characteristics of this material in its rolling and transverse rolling directions. The spread of characteristics within samples of the same orientation is small, e.g. in the case of the transverse samples, a maximum difference in magnetic field strength of 11 A/m at 1.8 T was observed between the 8 samples. The spread amongst the RD samples is more pronounced with a difference in magnetic field strength of 30 A/m at 1.8 T between the 8 samples.

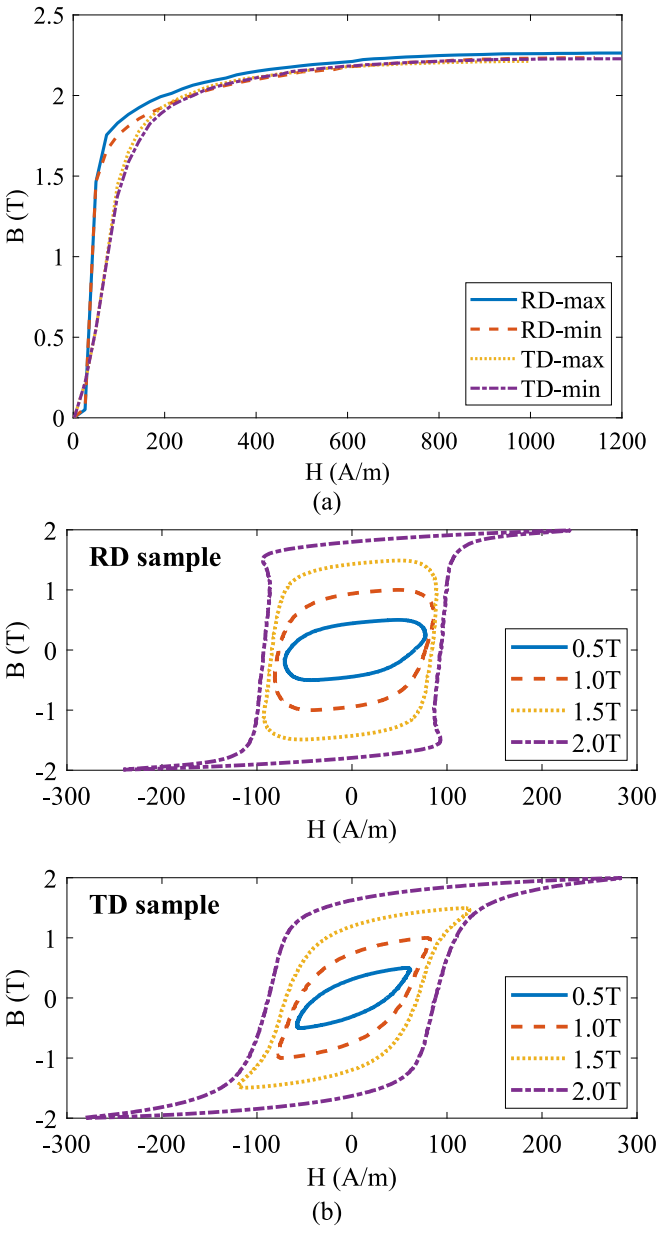

Fig. 5. Magnetization characteristics of RD samples and TD samples. (a) Maximum and minimum quasi-static magnetization curves. (b) Hysteresis loops at 400 Hz.

Fig. 4. Test rig for magnetization characterization. (a) Permeameter. (b) Single strip tester.

However, it should be noted that the edge damage effect model presented is based on establishing the change in permeability after laser cut in each individual sample against its own pre-cut characteristic rather than against a nominal or average characteristic. This gives some way to mitigating the influence of spread in characteristics of other nominally identical samples.

Following initial magnetic characterization of the strips, a series of samples with 1 to 4 slits shown in Fig. 6 were produced with a progressively increasing number of laser cuts along the lengths. The samples were cut by Tannlin UK Ltd using a 400 W rated laser operating at average power of 56 W with nitrogen gas assist and a 180 mm/s cutting rate. In each case, the cuts extended only over the central 290 mm of the strips leaving 5 mm uncut at each end as shown in Fig. 6. This joined section at each end was well outside the region whose properties contributed to the measured magnetic characteristics. The widths of the cuts were measured using a Keyence VHX-100 K digital microscope and the proportion of material removed was accounted for in the cross-section and mass used in the processing of the measured flux linkage and current data into B-H data.

The quasi-static magnetization curves measured with the single-strip tester for rolling direction samples with between 1 and 4 cuts are shown in Fig. 7 alongside the corresponding magnetization curves for an un-cut sample (designated as 0-slit). As would be expected, there is a progressive deterioration in the magnetization curve as more cuts are introduced in a sample of a given width. This data is useful in establishing the extent to which the damage is cumulative within these samples. It is worth noting that these 4 characteristics are for four samples, albeit from the same batch, and not for a single sample into which the introduction of individual cuts is interspersed with measurements.

A useful indicator of the cumulative nature of the degradation can be obtained from Fig. 8 which summarizes the variation with the number of slits of the magnitude of the magnetic field strength required to obtain a prescribed value of flux density. As will be apparent, there is a consistent and more-or-less linear increase in magnetic field strength required to achieve a given level of flux density as the number of slits increases, at least up to the 4 slits used in this test of measurements. This suggests that some degree of superposition can be applied to degradation from more than one cut, e.g. from the two cut edges on either side of a stator tooth body.

As expected, the relative permeability diminishes markedly with an increasing number of slits, as illustrated Fig. 9 in which the average relative permeability for each curve was derived from $B/(\mu_0 H)$.

The presence of a reversible region in the low flux density range is evident in each magnetization characteristic (typically up to 0.1 T or so), albeit that the limited resolution of the step-by-step sampling in this region causes some additional spread to that which would be expected from variations between different test-pieces alone. The reversible region of the magnetization curve where relative permeabilities of the order of 100 are encountered tends to be of limited interest in the modelling of high-performance electrical machines, although they are key in some sensor applications such as linear and rotary variable differential transformers [26] in which operation in the linear reversible region is key to their performance. Hence, it is commonplace in non-linear finite element modelling of high-performance electrical machines to set-aside the reversible region and, in many cases, approximate

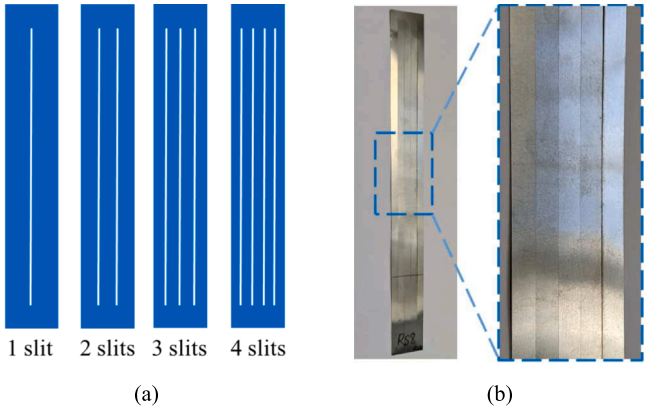

Fig. 6. Schematics and photo of slitted samples by laser cutting. (a) Schematics of slitted samples. (b) A 4-slit sample.

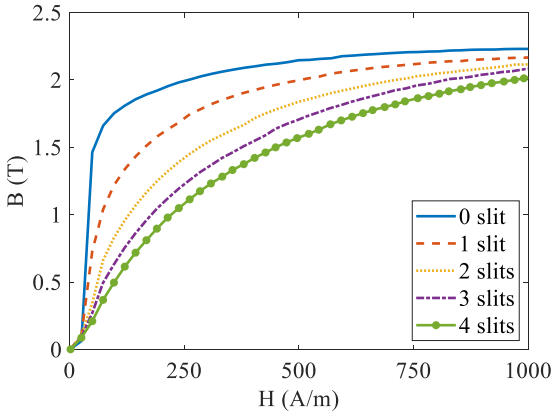

Fig. 7. Measured quasi-static magnetization curves with between 0 and 4 cuts for RD samples.

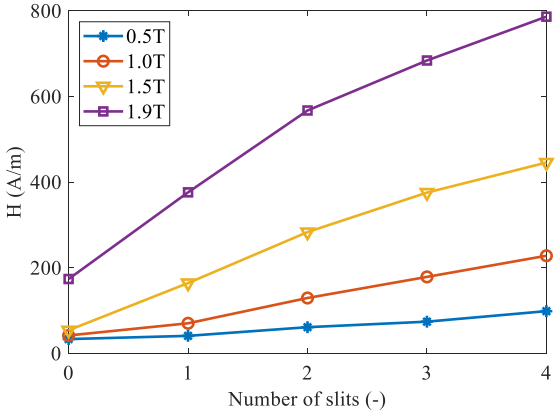

Fig. 8. Required magnetic field strength to obtain a prescribed value of flux density for the samples with various numbers of slits for RD samples.

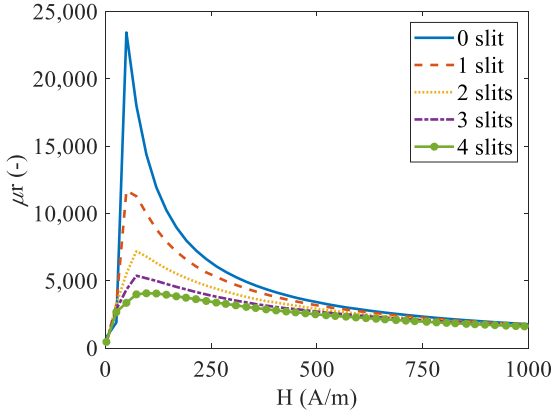

Fig. 9. Measured relative permeability curves with between 0 and 4 cuts for RD samples.

the magnetization curve with some form of analytical curve-fit function. Some functions have the advantage of enforcing both an incremental permeability of μ_0 at, and beyond, magnetic saturation and a monotonic rate of change in the permeability with magnetic field strength that aids stability and convergence of the iterative solution. Since the aim of the model being developed is to represent edge damage within a finite element representation of a machine, the function shown in (1) which is employed as one of several options for representing non-linear magnetization characteristics within the Altair FLUX suite of packages was used to curve fit the measured magnetization characteristics.

$$B(H) = \mu_0 H + J_s \frac{H_a + 1 - \sqrt{(H_a+1)^2 - 4H_a(1-\beta)}}{2(1-\beta)} \tag{1}$$

where $H_a = \mu_0 H(\mu_{r\_0} - 1)/J_s$, J_s represents the saturation flux density, β is knee adjustment coefficient, and μ_{r_0} is the initial relative permeability. Throughout this study, where Eq. (1) has been used to represent measured magnetization characteristics, the various coefficients have been established through minimization of the least squared errors using a trust-region type algorithm.

Fig. 10 and Fig. 11 show the magnetization characteristics and the variation of permeability with magnetic field strength respectively established through the application of Eq. (1) in combination with an optimization of its various coefficients. It is important to note that these characteristics in Fig. 10 are not material magnetization curves as such, but are mean flux density versus magnetic field strength for the specific geometry variant of the sample.

As would be expected, the relative permeabilities at low magnetic field strength region are affected markedly following curve-fitting using Eq. (1), although it represents the original behavior well over the vast majority of the characteristic. It is important to note that elimination of the reversible and lower permeability region is not a direct consequence of the representation of the edge-effect but is a common approach in the processing of experimental data for use in finite element packages.

3. Edge damage representation

A. *Mathematical model*

To account for the deterioration in the magnetization curve in the regions around the laser cut, a two-term exponential function was employed to represent the relative permeability reduction variation with the distance to the cut edge, as shown in (2).

$$\mu_r(x,H) = \left[1 - \left(ae^{bx} + ce^{dx}\right)\right]\mu_r(H) \tag{2}$$

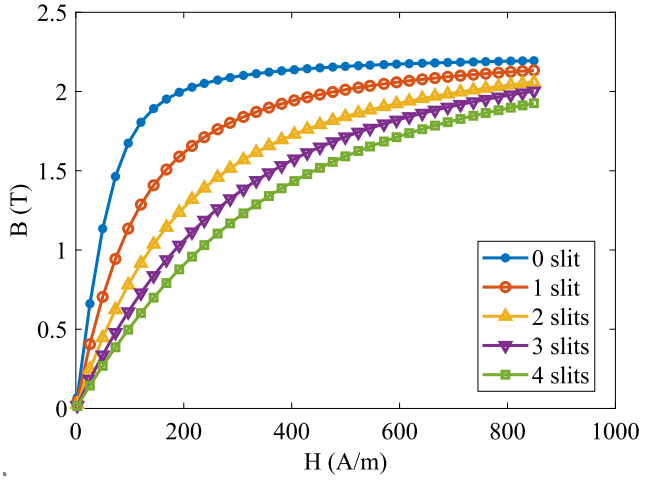

Fig. 10. Curve-fitted quasi-static magnetization curves derived from measurements with between 0 and 4 cuts for RD samples.

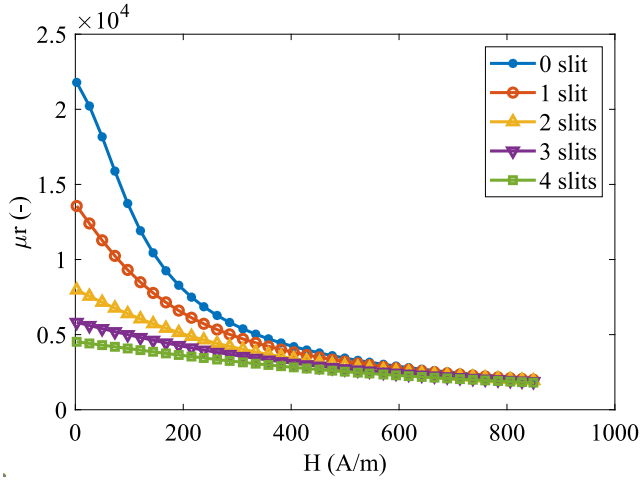

Fig. 11. Curve-fitted quasi-static relative permeability curves derived from measurements with between 0 and 4 cuts for RD samples.

where a, b, c, and d are coefficients of the relative permeability reduction function. x is the distance from the cut edge. $\mu_r(H)$ is the original permeability at a given value of magnetic field strength H.

When $x = 0$, $\mu_r = (1 - a - c)\mu_r(H)$. This edge condition sets some constraints on the range of values that can be taken by a and c if the permeability is to remain a positive number, i.e. $0 < a + c < 1$. As x increases, the nature of the function in Eq. (2) results in an increase in permeability towards the pristine value assumed to be measured on a test-piece with no damage. The rate of the increase is determined by the double exponential. The use of double exponentials provides a greater degree of control over the shape of the variation as compared to a single exponential. In order to provide the necessary decay of the exponents, $b < 0$ and $d < 0$. However, on inspection it can be seen that the ae^{bx} term and ce^{dx} term have same form and hence the coefficients are interchangeable while still producing the same result. To ensure a unique solution to the best curve fit and hence avoid solving badly conditioned equations, an additional constraint of $b > d$ is imposed. In summary, the a-priori constraints imposed on the edge damage function in (2) are:

$$\begin{cases} 0 < a + c < 1 \\ d < b < 0 \end{cases} \tag{3}$$

Equation (2) represents the relative permeability variation with distance away from a cut edge. However, any laser cut within the strip will generate damage in both directions away from the cut. Hence, Eq. (2) must be applied in both directions away from the strip. As a

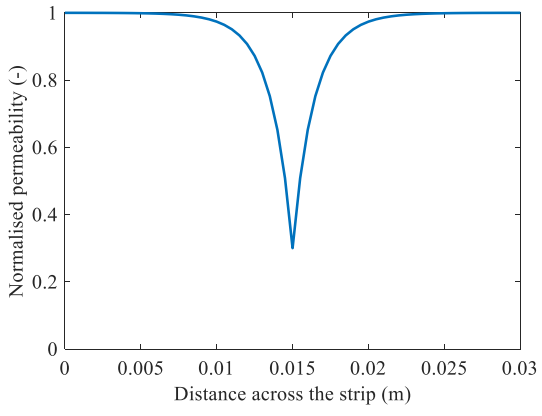

Fig. 12. Variation in normalized permeability across one strip due to a single cut along the mid-line of the strip ($a = 0.5$, $b = -600$, $c = 0.2$ and $d = -1000$).

representative example, Fig. 12 shows the normalized variation of permeability across one strip due to a single slit along the mid-line of the strip for the arbitrary and illustrative set of coefficients: $a = 0.5$, $b = -600$, $c = 0.2$ and $d = -1000$.

The spatial variation in the permeability will give rise to a corresponding spatial flux density variation across the width of the strip when a given magnetic field strength is applied. However, the variation in the flux density across the width of the strip cannot be directly measured and the sole measurement available is the total flux in the sample, which in turn provides a means of inferring an average flux density in the sample. It is necessary to integrate the flux density contributions from across the strip:

$$B_{mean}(W,H) = \frac{1}{W}\int_0^W \mu_0 H \mu_r(x,H)dx \tag{4}$$

where W is the strip width, and μ_0 is the permeability of free space.

As further slits are added into a strip, it is important to establish a consistent representation of the cumulative damage done to the material. The representation adopted in this model is straightforward and represented by the product of the individual functions for degradation associated with each cut.

For a very spatially rapid recovery of permeability, i.e. a small effective depth of damage which would correspond to large absolute values of the parameters b and d in Eq. (2), successive cuts will barely interact and the cumulative effects in any region would be small. By way of an illustrative example, Fig. 13 shows the individual functions for two cuts at 10 mm and 20 mm across the width of a 30 mm strip and a combined variation which is simply the product of the two individual variations with the same set of parameters as Fig. 12.

Whereas taking the product of the individual functions from two cuts may be sufficient to represent the cumulative effects in a region such as a tooth body of an electrical machine stator core, in its simplest form it cannot account for the multi-cut test samples shown previously in Fig. 6. In this case, the cuts are introduced with successive passes of the laser and hence different regions would be exposed to different levels of heat-soak from the cut depending on whether that region was already separated from the region being cut by the laser.

Taking as an example the strip with four cuts shown previously in Fig. 6 and assuming that the cuts were done sequentially from left to right. The first cut would result in some degradation in the narrow region to the left of the cut and into the remainder of the sample to the right of the cut, albeit that the extent of the damage in regions more remote from the cut would depend on the parameters b and d. When the second cut in from the left edge is done, then the region to the immediate left of this second cut is subjected to further accumulated damage as is the remainder of the strip to the right of the cut. However, the region of the strip to the left of the first cut is not connected to the region in which the second cut is being made (by virtue of the presence of the first cut) and hence it seems reasonable to assume that this region does not suffer any further accumulated damage from the second cut. Hence, the accumulation of damage builds up from left to right across the strip and progressively areas become separated from the thermal effects of successive cuts. The extent to which this asymmetrical damage builds up depends on the effective depth of the damage from a given cut. For example, using the same parameter set as that used for Fig. 12 and Fig. 13 and applying this cumulative approach with regions gradually becoming separated leads to the representation shown in Fig. 14 for a 30 mm strip with four cuts. As will be apparent, in this case there is relatively little asymmetry since the separation of the 4 cuts is 6 mm which is close to the effective damage depth shown in Fig. 12.

In contrast, if the parameters b and d are reduced to -200 and -500 respectively with a and c remaining at 0.5 and 0.2 respectively, the depth of the spatial extent of effective damage is greatly increased compared to the previous parameter set, as shown in Fig. 15 for the case of a single symmetrical cut along the mid-line of the strip. As will be evident, there is appreciable damage from this single cut at the edges of the 30 mm wide strip the full strip. This rather extreme case, which is not necessarily representative of damage encountered in practice, nevertheless serves to illustrate the importance of the cutting order in a multi-cut strip of the type being used for characterizing the edge damage in this study.

Applying cumulative damage methodology based on progressive multiplication of individual cut effects with regions gradually becoming separated leads to the predicted variation in permeability across a 30 mm strip with 4 cuts shown in Fig. 16, again with the same parameters of 0.5, -200, 0.2 and -500 for a, b, c and d respectively. As will be apparent, even with a parameter set that gives rise to a large zone of damage, the asymmetry across the strip, although discernable, remains modest.

4. Model parameter fit to measured data

The preceding examples of parameter sets were arbitrary and intended to demonstrate the underlying features and behavior of the model. Ultimately, it is necessary to use measurements from test-pieces to establish a set of parameters for the model which fits a specific combination of material and cutting conditions at a given value of magnetic field strength. In the model adopted, there are four parameters which define the nature of the edge damage variation and hence four independent measurements of effective permeability are required. It is important to recognize that whereas this in principle provides sufficient data points to eliminate the four unknowns, it is not a given that the measurement will provide a well-conditioned set of equations that yield

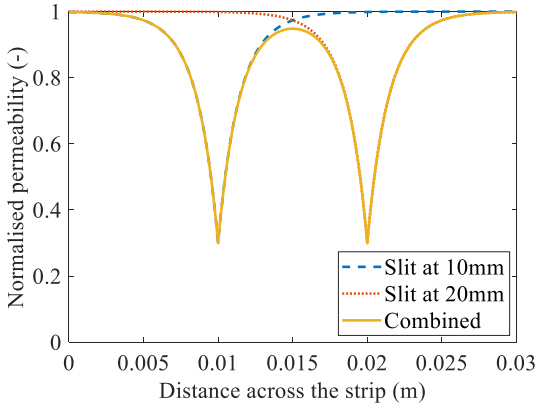

Fig. 13. Variation in normalized permeability across one strip due to two slits ($a = 0.5$, $b = -600$, $c = 0.2$ and $d = -1000$).

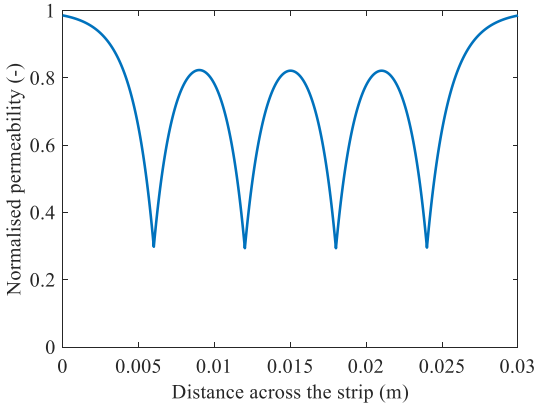

Fig. 14. Variation in normalized permeability across one strip due to four slits ($a = 0.5$, $b = -600$, $c = 0.2$ and $d = -1000$).

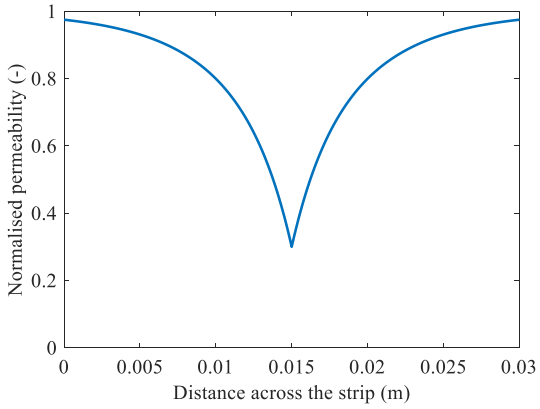

Fig. 15. Variation in normalized permeability across one strip due to a single cut along the mid-line of the strip ($a = 0.5$, $b = -200$, $c = 0.2$ and $d = -500$).

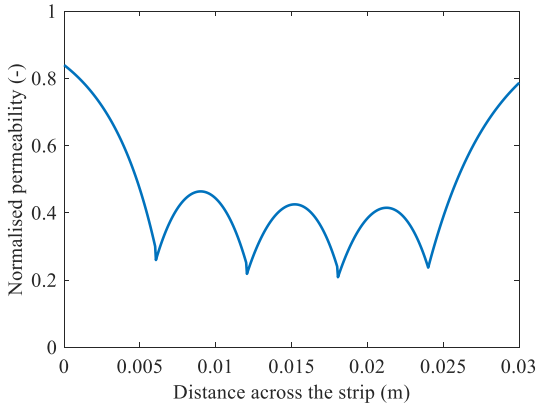

Fig. 16. Variation in normalized permeability across one strip due to four slits ($a = 0.5$, $b = -200$, $c = 0.2$ and $d = -500$).

a well-defined and unique set of parameters.

The least square error method was employed to determine a, b, c and d coefficients at various magnetic field strengths, by minimizing the mean error between the predicted and measured permeabilities for all the slitted samples. The resultant a, b, c and d coefficients as a function of magnetic field strength are illustrated in Fig. 17. It can be observed that those coefficients largely depend on the magnetic field strength, and hence the magnetic field strength effect on the edge damage effect is marked and should be taken into account when implementing the edge damage model in finite element analysis. It can also be seen that the difference between b and d is relatively small, indicating a possibility of using a single exponential term to model the edge damage effect for the Cobalt-iron alloy used in this paper. However, the two exponential terms with different decay rates do provide more degree of freedoms when modelling other materials and/or other cutting techniques. Therefore, this paper still pursues a model with two exponential terms to represent the edge damage.

5. Generation of layered magnetization curves

The model derived in section III and parameterized for a particular combination of material and cutting conditions provides a means of mapping edge damage, from one or more cuts, onto a finite element model of a stator or rotor core. However, as current configured the model represents a continuous variation which allows the permeability to be estimated at a given combination of magnetic field strength and distance from the edge. In a finite element package with full access to the solver, such as in-house code or a flexible tool such as COMSOL, it may

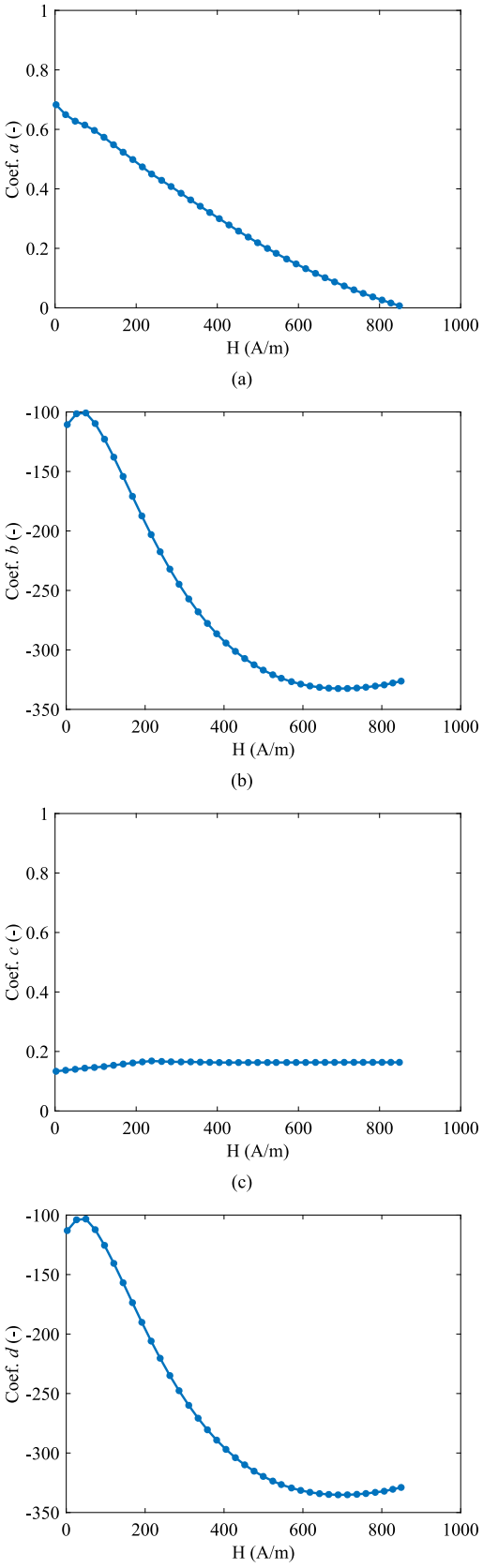

Fig. 17. Derived edge damage model coefficients based on measured magnetization curves of rolling direction samples.

be possible to integrate this model such that it can be applied on element-by-element basis. However, commercial finite element packages tend to dominate everyday use for research and product development. One means of integrating a spatial permeability variation model into a finite element model in a commercial package with limited or no access to the solver is to divide the core region into a series of discrete layers, each of which is regarded as a distinct region with its own magnetization curve [16]. These individual layers can, at least in principle, be as narrow as a single finite element depth.

In order to adopt such a layered model, it is necessary to use the model developed in section III with a full set of parameters derived from measurements to generate a series of magnetization curves in which the distance to the edge is set at mean distance of the inner and outer profiles of the layer. It is important to note that this process must take account of all the laser cuts which might impact on the net magnetization characteristics, recognizing that the effects of cuts close to the layer may well dominate over more distance cuts. For the parameters established for Hiperco 50 with the laser cutting conditions set out in section II, the first ten resulting magnetization curves in 10 mm thick layers are shown in Fig. 18 for the rolling direction samples. The particular case shown is for the idealized case of a single cut in which it is assumed that the distance to any further cuts is sufficient to make their contribution negligible.

6. Experimental validation of the model

In order to validate the model a further 4 test-pieces were cut from the center of 30 mm wide strips of the same batch of Hiperco 50 (both rolling direction and transverse direction samples) and using the same laser cutting condition. These test-pieces were 8 mm, 10 mm, 12 mm and 14 mm wide strips which spanned the full length of the 300 mm long strips from which they were taken. The effective quasi-static magnetization curves of these four rolling direction strips were measured in the single-strip tester and are shown in Fig. 19 alongside the corresponding characteristic for a 30 mm wide reference strip from the same batch. In all cases, the B axis corresponds to the effective mean flux density. As will be apparent, there is a marked difference in the effective magnetization curves of these 4 strips, which is indicative of different relative contributions to the net characteristic from damaged regions. As would be expected, the 14 mm wide shows the least degradation in its overall effective magnetization characteristic from the starting 30 mm wide strip.

One-dimensional finite element models of each strip were established in which each strip was divided into 0.1 mm wide layers in order to represent the spatial variation in permeability away from the cut edges. The resulting predicted net magnetization characteristics are shown in Fig. 20 alongside the corresponding measured effective characteristics. As will be apparent, there is good agreement in terms of the

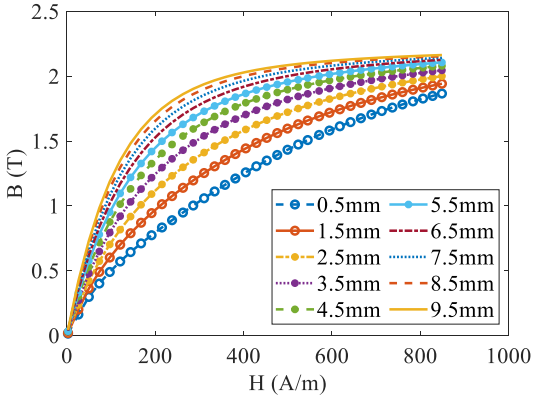

Fig. 18. Generated layered magnetization curves based on the edge damage model of rolling direction samples for 10 mm thick layers.

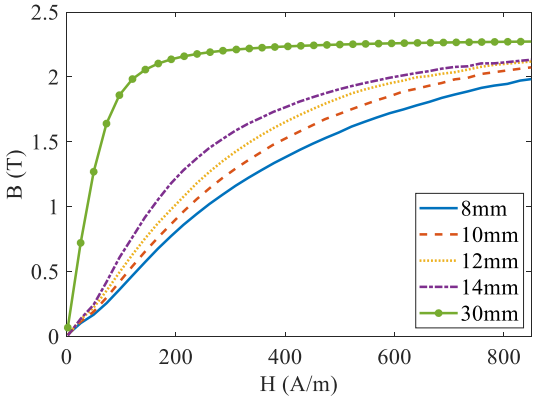

Fig. 19. Measured quasi-static magnetization curves of 8 mm, 10 mm, 12 mm and 14 mm wide rolling direction strips alongside the 30 mm wide reference strip before cut.

predictions and measured behavior of the strips, in particular that the model captures well the significant degradation introduced by laser cutting from the reference 30 mm wide strip that has no cuts present.

It is worth noting that while the original pre-cut characteristic and the predicted characteristic from the edge damage model do not contain a reversible region by virtue of having been fitted using the expression in Eq. (1), the measured characteristic is the raw measured data which has undergone no such fitting. There is therefore a contribution to the discrepancies observed in Fig. 20 from the comparison of a fitted curve with an actual measured curve with an appreciable reversible region.

It is interesting to note that there is significant variation in the flux density across the strip widths. By way of example, Fig. 21 shows the predicted variation in flux density across the 8 mm wide rolling direction strip at three discrete values of magnetic field strength. This redistribution flux across a sample due to edge damage may play an important role in increasing the core loss in a given region since the loss is proportional to something akin to the square of the flux density. Note that the redistribution effect on the core loss may be subject to the flux densities and frequencies. It is important to recognize that this flux redistribution effect is in addition to any changes in the localized loss behavior when subjected to a specific level of excitation, i.e. edge damage causing a localized change in the loss model coefficients. This latter aspect is not considered in this investigation but is undoubtedly an important topic for future research, albeit one that is extremely challenging.

7. Conclusion

This paper proposes an edge damage effect model with normalized permeability as a function of both the distance to cut edge and the magnetic field strength, to account for the permeability changes in electrical steels due to laser cutting. Although undertaken within the context of the relatively neglected material system of Cobalt-iron, it has read-across to other materials such as Silicon-iron. Compared to the existing models in literature, the proposed model accounts for the magnetic field strength effect and the accumulative edge damage effect simultaneously, and hence it is contended that it provides an enhanced representation of the edge damage effect on the material magnetization curves. The proposed model can be implemented by either multi-layer material model or continuous material model in finite element analysis. The modelling of the edge damage effect on the core loss of Cobalt iron alloys will be performed in the future work.

CRediT authorship contribution statement

Xiao Chen: Conceptualization, Methodology, Software, Writing –

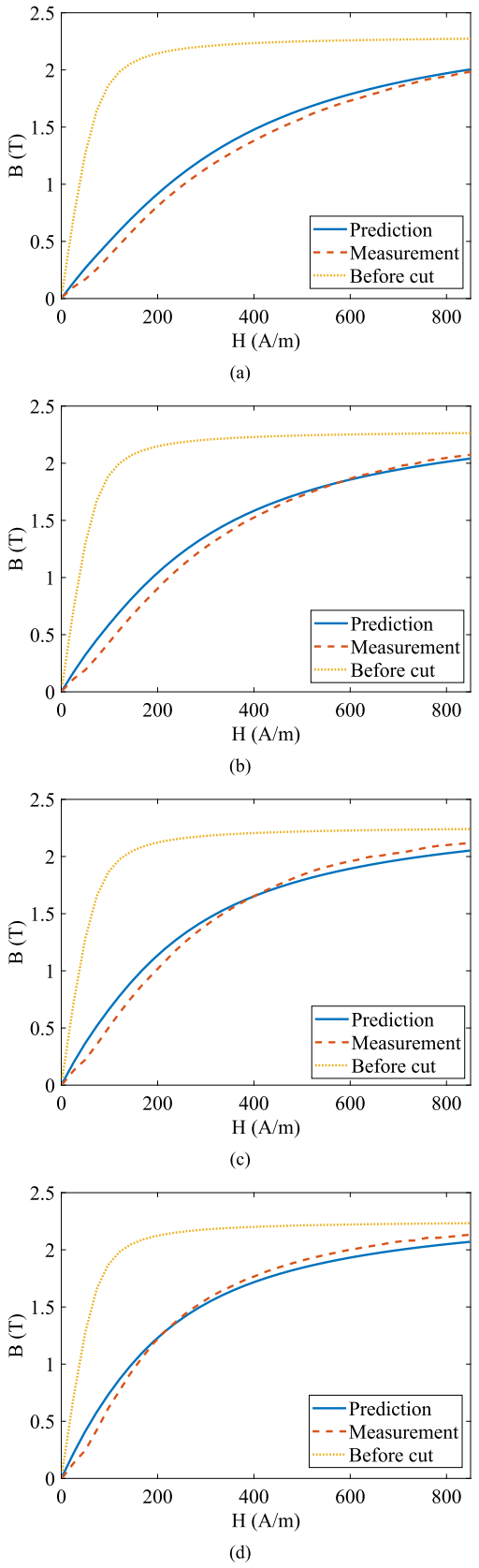

Fig. 20. Comparison of the model predicted and measured quasi-static magnetization curves of 8 mm, 10 mm, 12 mm and 14 mm wide rolling direction strips alongside the 30 mm wide reference strip before cut. (a) 8 mm wide strip. (b) 10 mm wide strip. (c) 12 mm wide strip. (d) 14 mm wide strip.

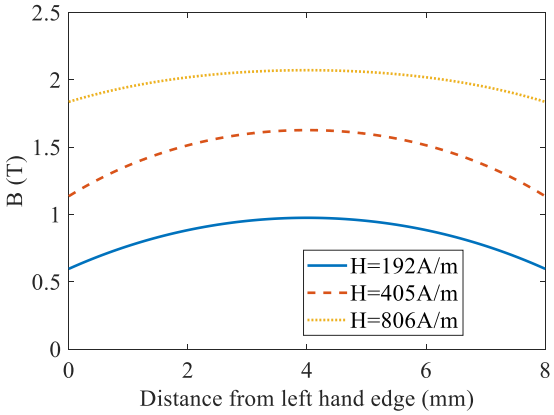

Fig. 21. Predicted variation in flux density across the width of the 8 mm rolling direction strip at 3 discrete values of magnetic field strength.

original draft, Project administration. **Han Wu:** Data curation, Formal analysis, Investigation, Validation, Visualization. **Jason D. Ede:** Methodology, Investigation, Validation, Writing – review & editing. **Geraint W. Jewell:** Conceptualization, Supervision, Writing – review & editing, Funding acquisition, Resources, Project administration. **Luke M. Jones:** Methodology, Investigation, Validation, Visualization, Writing – review & editing. **Hassan Ghadbeigi:** Supervision, Investigation, Validation, Writing – review & editing, Resources, Project administration.

Declaration of Competing Interest

The authors declare the following financial interests/personal relationships which may be considered as potential competing interests: Geraint Jewell reports financial support was provided by EPSRC Future Electrical Machines Manufacturing Hub. Geraint Jewell reports equipment, drugs, or supplies was provided by Carpenter Technology Corporation.

Data availability

The data that has been used is confidential.

Acknowledgments

This work is supported by the UK Engineering and Physical Sciences Research Council (EPSRC) through funding for the Future Electrical Machines Manufacturing Hub (Award EP/S018034/1). The authors would like to acknowledge Carpenter Technology for their supply and heat treatment of the samples used in this investigation.

References

[1] J. Powell, CO2 Laser Cutting, Springer, London, 1998.
[2] H. Naumoski, B. Riedmüller, A. Minkow, U. Herr, Investigation of the influence of different cutting procedures on the global and local magnetic properties of non-oriented electrical steel, J. Magn. Magn. Mater. 392 (2015) 126–133.
[3] A. Schoppa, H. Louis, F. Pude, C. von Rad, Influence of abrasive waterjet cutting on the magnetic properties of non-oriented electrical steels, J. Magn. Magn. Mater. 254–255 (2003) 370–372.
[4] E.C. Jameson, Electrical Discharge Machining, Society of Manufacturing Engineers, 2001.
[5] M. Hubert, J. Franke, Rotary cutting of electrical steel laminations—an innovative method for manufacturing electrical machines, Electr. Power Compon. Syst. 44 (9) (2016) 1071–1074.
[6] P. Jeżowski, M. Nowicki, M. Grzeszkowiak, R. Czajka, F. Béguin, Chemical etching of stainless steel 301 for improving performance of electrochemical capacitors in aqueous electrolyte, J. Power Sources 279 (2015) 555–562.
[7] S. GmbH, Metal Forming Handbook, Springer-Verlag, 1998.
[8] M. Emura, F.J.G. Landgraf, W. Ross, J.R. Barreta, The influence of cutting technique on the magnetic properties of electrical steels, J. Magn. Magn. Mater. 254–255 (2003) 358–360.

[9] F. Wu, L. Zhou, J. Soulard, B. Silvester, C. Davis, Quantitative characterisation and modelling of the effect of cut edge damage on the magnetic properties in NGO electrical steel, J. Magn. Magn. Mater. 551 (2022), 169185.
[10] S. Steentjes, G. von Pfingsten, K. Hameyer, An application-oriented approach for consideration of material degradation effects due to cutting on iron losses and magnetizability, IEEE Trans. Magn. 50 (11) (2014) 1–4.
[11] P. Lazari, K. Atallah, J. Wang, Effect of laser cut on the performance of permanent magnet assisted synchronous reluctance machines, IEEE Trans. Magn. 51 (11) (2015) 1–4.
[12] H. Wang, Y. Zhang, Modeling of Eddy-current losses of welded laminated electrical steels, IEEE Trans. Ind. Electron. 64 (4) (2017) 2992–3000.
[13] K. Yamazaki, W. Fukushima, Loss analysis of induction motors by considering shrink fitting of stator housings, IEEE Trans. Magn. 51 (3) (2015) 1–4.
[14] S. Elfgen, S. Steentjes, S. Böhmer, D. Franck, K. Hameyer, Influences of material degradation due to laser cutting on the operating behavior of PMSM using a continuous local material model, IEEE Trans. Ind. Appl. 53 (3) (2017) 1978–1984.
[15] S. Elfgen, P. Rasilo, K. Hameyer, Hysteresis and eddy-current losses in electrical steel utilising edge degradation due to cutting effects, Int. J. Numer. Model. Electron. Networks Devices Fields 33 (5) (2020) e2781.
[16] Z. Gmyrek, A. Cavagnino, L. Ferraris, Estimation of the magnetic properties of the damaged area resulting from the punching process: Experimental research and FEM modeling, IEEE Trans. Ind. Appl. 49 (5) (2013) 2069–2077.
[17] T.P. Holopainen, P. Rasilo, A. Arkkio, Identification of magnetic properties for cutting edge of electrical steel sheets, IEEE Trans. Ind. Appl. 53 (2) (2017) 1049–1053.
[18] L. Vandenbossche, S. Jacobs, X. Jannot, M. McClelland, J. Saint-Michel, E. Attrazic, Iron loss modelling which includes the impact of punching, applied to high-efficiency induction machines, in: *2013 3rd International Electric Drives Production Conference (EDPC)*, 29-30 Oct. 2013 2013, pp. 1-10.
[19] N. Alatawneh, A. Saleem, T. Rahman, D.A. Lowther, R. Chromik, Modelling and analysis of the effects of cutting of core laminations in electric machines, IET Electr. Power Appl. 14 (12) (2020) 2355–2361.
[20] L. Vandenbossche, S. Jacobs, F. Henrotte, K. Hameyer, Impact of cut edges on magnetization curves and iron losses in e-machines for automotive traction, World Electric Veh. J. 4 (3) (2010) 587–596.
[21] S. Elfgen, S. Steentjes, S. Böhmer, D. Franck, K. Hameyer, Continuous local material model for cut edge effects in soft magnetic materials, IEEE Trans. Magn. 52 (5) (2016) 1–4.
[22] N. Leuning, S. Elfgen, B. Groschup, G. Bavendiek, S. Steentjes, K. Hameyer, Advanced soft- and hard-magnetic material models for the numerical simulation of electrical machines, IEEE Trans. Magn. 54 (11) (2018) 1–8.
[23] R. Siebert, J. Schneider, E. Beyer, Laser cutting and mechanical cutting of electrical steels and its effect on the magnetic properties, IEEE Trans. Magn. 50 (4) (2014) 1–4.
[24] M. Bali, A. Muetze, The degradation depth of non-grain oriented electrical steel sheets of electric machines due to mechanical and laser cutting: A state-of-the-art review, IEEE Trans. Ind. Appl. 55 (1) (2019) 366–375.
[25] H. Ahlers, J.D. Sievert, Q.C. Qu, Comparison of a single strip tester and Epstein frame measurements, J. Magn. Magn. Mater. 26 (1) (1982) 176–178.
[26] G.W. Midgley, D. Howe, P.H. Mellor, An assessment of alternative soft magnetic materials in rotary variable differential transformers, J. Appl. Phys. 81 (8) (1997) 4295–4297.